

# A Charge Density Wave-like Transition in High Temperature Quenched $\text{Bi}_2\text{Se}_3$

Yanan Li<sup>1</sup>, Christian Parsons<sup>1</sup>, Sanath Ramakrishna<sup>2</sup>, Anand Dwivedi<sup>1</sup>, Marvin Schofield<sup>1</sup>, Arneil Reyes<sup>2</sup>, and Prasenjit Guptasarma<sup>1\*</sup>

<sup>1</sup>Department of Physics, University of Wisconsin-Milwaukee, Milwaukee, Wisconsin 53211, USA

<sup>2</sup>National High Magnetic Field Laboratory/Florida State University, Tallahassee, Florida 32310, USA

E-mail: yananli@uwm.edu

Received xxxxxx

Accepted for publication xxxxxx

Published xxxxxx

## Abstract

Hexagonally deformed Fermi surfaces and strong nesting, found in topological insulators (TIs) such as  $\text{Bi}_2\text{Se}_3$  and  $\text{Bi}_2\text{Te}_3$ , have led to several predictions of the existence of Density Wave order in these systems. Recent evidence for strong Fermi surface nesting in superconducting  $\text{Cu-Bi}_2\text{Se}_3$  and  $\text{Nb-Bi}_2\text{Se}_3$  has further led to speculation about the importance of charge order in the context of unconventional superconductivity. Here, we report the first observation of a novel anomaly in  $\text{Bi}_2\text{Se}_3$  at 140K, which may be associated with a Charge Density Wave (CDW)-like transition. This transition was identified from both structural and electronic measurements, where: a) a periodic lattice distortion at above room temperature was characterized as a diffuse charge order in  $\text{Bi}_2\text{Se}_3$  between  $\vec{k}$  and  $\vec{k} \pm \Delta\vec{k}$  from electron diffraction; and b) an opening of energy gap signified with metal-to-insulator like transition at 140K was identified from resistivity vs temperature measurement. This is further corroborated by nuclear magnetic resonance (NMR) studies of the spin-lattice relaxation ( $1/T_1$ ) rate of the  $^{209}\text{Bi}$  nucleus, which also displays a transition at 140K associated with an opening of an energy gap of  $\sim 8\text{meV}$ . Additionally, we also observe another anomaly in  $1/T_1$  near 200K, which appears to display anisotropy with the direction of the applied magnetic field.

Keywords: Topological Insulator,  $\text{Bi}_2\text{Se}_3$ , Charge Density Wave, Phase Transition, Fermi surface Nesting, Lattice Distortion, Intercalation, Electron-phonon Coupling

## 1. Introduction

The 2D layered chalcogenide  $\text{Bi}_2\text{Se}_3$  and its intercalated versions continue to elicit significant interest due to the presence of non-trivial topological surface states protected by time-reversal symmetry, along with fascinating properties of nematic order and superconductivity [1-6]. Ideally,  $\text{Bi}_2\text{Se}_3$  is a 3D topological insulator with a single Dirac cone within a substantial bulk energy gap (0.3 eV) [7]. However, several experiments have

observed a lowering of the bulk conduction band due to natural electron doping from vacancies or antisite defects crossing the Fermi energy and allowing for bulk electron conduction [8-11]. Under high pressure, or upon intercalating with metals such as Cu and Nb,  $\text{Bi}_2\text{Se}_3$  displays unconventional superconductivity [12-14]. Most unconventional superconductivity arises from strong electron-electron correlations [15-18]. However,  $\text{Bi}_2\text{Se}_3$  displays weak *sp* electron correlation [19, 20]. This conundrum has led to a search for other possible

mechanisms for unconventional electron pairing in Cu-, Sr- and Nb- intercalated  $\text{Bi}_2\text{Se}_3$ . An idea that has gained ground in recent years is based on Fermi surface nesting. First-principles calculations on  $\text{Cu}_x\text{Bi}_2\text{Se}_3$ , in combination with elastic neutron diffraction measurements on  $\text{Sr}_{0.1}\text{Bi}_2\text{Se}_3$ , indicate that singular electron-phonon interactions with strong Fermi surface nesting at long wavelength can lead to pseudo-triplet pairing with  $A_{2u}$  symmetry [1, 2]. In addition to this, there is now strong evidence that with contributions from the bulk, the cross-section of the Dirac cone in  $\text{Bi}_2\text{Se}_3$  evolves from circular geometry at the Dirac point into a hexagon-like geometry around 350 meV above the Dirac point, and eventually to a hexagram-like geometry near 435 meV above the Dirac point [21]. The near-flat pieces of such a hexagon in the range  $0.55E^* < E < 0.9E^*$  can result in nesting vectors at  $Q_i = 2k_{\text{Fe}i}$ ,  $i=1\dots3$ , where  $Q_i$  is the wave vector and  $k_{\text{Fe}i}$  is the Fermi momentum [22]. Central to a strong Fermi surface nesting factor is the layered structure of  $\text{Bi}_2\text{Se}_3$ . Angle-resolved Photoemission Spectroscopy (ARPES) studies on  $\text{Bi}_2\text{Se}_3$  have confirmed that natural electron-doped  $\text{Bi}_2\text{Se}_3$  has a hexagonally deformed Fermi Surface. Kuroda et al. have suggested that two flat segments of a hexagonal Fermi surface facing each other across  $2\vec{k}_F$  along  $\vec{\Gamma} - \vec{k}$  could lead to strong nesting [21]. One of the possible outcomes of such Fermi surface nesting is the appearance of Density Waves. Realistically, this is a deviation from an ideal Topological Insulator (TI), which has a single Dirac cone with a circular Fermi surface [23], and in which the formation of a charge density wave, or a spin density wave, is forbidden. A few studies have hinted at the existence of CDWs in Cu- $\text{Bi}_2\text{Se}_3$ , but so far there has been no evidence of a gap opening with temperature variation, indicating a CDW transition [24-26]. Additionally, there have been no such reports in  $\text{Bi}_2\text{Se}_3$ . Here, we report for the first time that  $\text{Bi}_2\text{Se}_3$  undergoes a transition to a possible CDW state at 140K.

The ground state of a charge density wave (CDW), observed mostly in low-dimensional materials, is

characterized by spontaneously broken translational symmetry. In more complex systems, the phase transition to a CDW ground state is mostly observed together with commensurate/incommensurate Periodic Lattice Distortions (PLD) concomitant with the opening of an energy gap at the Fermi level, resulting in a metal-to-insulator like transition as a function of temperature [27,28].

We report here a combination of resistivity, Selected Area Electron Diffraction (SAED) and Nuclear Magnetic Resonance (NMR) studies to argue that  $\text{Bi}_2\text{Se}_3$  undergoes a transition to a possible CDW state at 140K. We observe a 140K metal-to-insulator like transition in resistivity as a function of temperature. Our measurements of the NMR spin-lattice relaxation ( $1/T_1$ ) rate of the  $^{209}\text{Bi}$  nucleus also shows an anomaly at 140K, which can be fitted to an energy gap of approximately 8meV. Additionally, electron diffraction reveals a periodic lattice distortion (PLD) in  $\text{Bi}_2\text{Se}_3$  as well as diffuse charge order between  $\vec{k}$  and  $\vec{k} \pm \Delta\vec{k}$ , as described in the previous paragraph. We argue that this diffuse scattering arises from an incommensurate charge density wave (I-CDW) at a higher temperature, foreshadowing a transition to CDW order, into which the I-CDW locks upon cooling below  $\sim 140\text{K}$ . We also identify evidence of another anomaly in NMR  $1/T_1$  near 200K which is anisotropic with applied magnetic field. Comparison of relaxation rates  $\Delta 1/T_1$  from  $\text{H}\parallel\text{c}$  to  $\text{H}\perp\text{c}$ , with  $\Delta 1/T_1 = 1/T_1(\parallel) - 1/T_1(\perp)$ , again signifies this transition indicating that a stronger lattice vibration (phonons) is present in the  $\text{H}\parallel\text{c}$ -axis measurements. Therefore, it is likely that the transition at 200K is a phonon-mediated structural phase transition.

## 2. Method

Single crystals of  $\text{Bi}_2\text{Se}_3$  were prepared by melting high-purity (99.999%) powders of Bi and Se. Stoichiometric mixtures of 2.5 g were sealed into high-quality quartz tubes in vacuum after being weighed and sealed in an inert glove box, taking extreme care never to expose to air. The mixtures sealed in quartz tubes were heated up to 850 C and

held for 20 hours. They were then cooled to 650 C at 0.1 C/min, followed by quenching from high temperature into ice water. This yielded large, shiny single crystals which were easily cleaved along the ab plane.

Powder X-ray diffraction data were collected from pieces of single crystals powdered inside an inert glove box. Rietveld refinement was performed using GSAS (General Structure Analysis System) and the EXPGUI interface. Selected Area Electron Diffraction (SAED) was performed at room temperature with a Hitachi H-9000NAR high-resolution transmission electron microscope (HRTEM) operated at 300 kV. Four-probe resistivity measurements were performed with a rate of 1K/step at varying temperatures and magnetic fields using a Quantum Design Physical Property Measurement System (PPMS).

Pulsed  $^{209}\text{Bi}$  NMR (Nuclear Magnetic Resonance) measurements were performed on a  $\text{Bi}_2\text{Se}_3$  single crystal of crystal size  $\sim 0.94 \times 0.58 \times 0.41$  cm placed inside a home-built probe in an 11-Tesla Helium cryostat. The single crystal of  $\text{Bi}_2\text{Se}_3$  was studied with the magnetic field oriented in two directions,  $H \perp c$  and  $H \parallel c$ . Field sweep spectrums were performed at frequency  $f=67.875\text{MHz}$ . Spin-echo signals for  $^{209}\text{Bi}$  NMR spectra were processed using the summed Fourier transform method, with the field swept from 9.7T to 10.5T. Spin Lattice relaxation time  $T_1$  measurements in both  $H \parallel C$  and  $H \perp C$  ( $H=9.86\text{T}$ ) directions were performed at stabilized temperature points varying between 1.6K and 300K. We employed a train of RF pulses on the central transition to saturate the magnetization followed by variable delays and integrate the spin-echoes to map the magnetization recovery.

The magnetization recovery  $M(t)$  is fitted with a stretched single exponential, appropriate for the initial condition where the quadrupolar satellites are completely saturated [29]:

$$M(t) = M_{\infty} \left[ 1 - e^{-(t/T_1)^{\beta}} \right] \quad (1)$$

where the parameter  $\beta$  allows for a distribution of  $T_1$ . Magnetization recovery  $M(t)$  can either be fitted by a master equation or a stretched exponential

equation [29, 30]. Stretched exponential fitting is used when there is a continuous distribution of relaxation rates. We used a pulse train to saturate all the NMR lines in our measurement set-up. Although the signal does not saturate completely, we find that a stretched single exponential fits our data better than the master equation.

### 3. Results

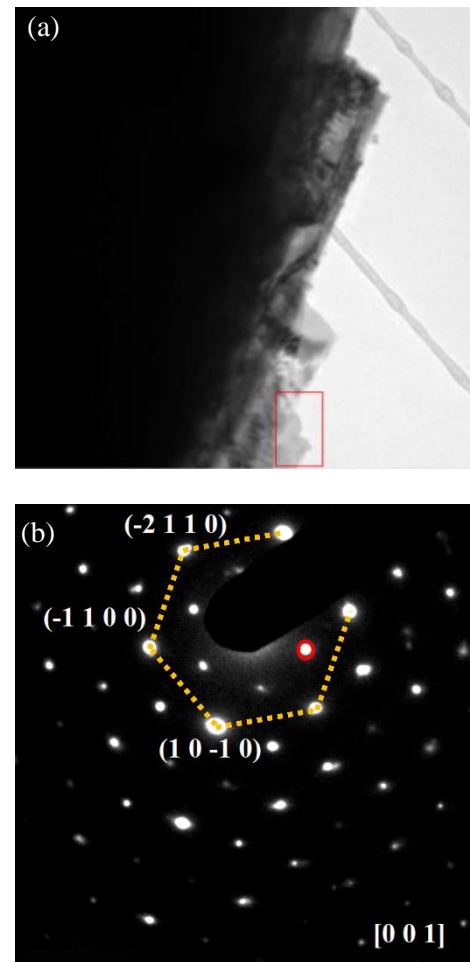


**Figure 1** Transmission Electron Microscopy (TEM) and Selected Area Electron Diffraction (SAED) studies on  $\text{Bi}_2\text{Se}_3$  single crystal at room temperature. (a) Bright-field image of a piece from a single crystal of  $\text{Bi}_2\text{Se}_3$ . The red box indicates the region on which SAED was performed. (b) Electron diffraction along [001] zone axis. Weak reflections of the type identified by a red circle represent normally forbidden reflections from  $3a/2$

#### 3.1 Structural study

Figure 1 and Figure 2 show Selected Area Electron Diffraction (SAED) performed on  $\text{Bi}_2\text{Se}_3$  at room temperature. Figure 1a shows the area from which the diffraction pattern in Figure 1(b) was

obtained along the [001] zone axis. Note the alternate bright and dim spots in Figure 1(b), with high-intensity spots identified and connected with yellow dash-lines. These features were also observed in SAED by Koski et al. and Wang et al. [24, 31]. Both groups studied the results of the intercalation of different zero-valent metals into the van der Waals gaps in  $\text{Bi}_2\text{Se}_3$ . They suggest that the most likely reason for the appearance of these weak intensity spots, otherwise forbidden in the cubic-like ABC [001] zone axis in the host  $\text{Bi}_2\text{Se}_3$  lattice, is the result of a stacking fault. In other words, the presence of zero-valent intercalants in the van der Waals gap can alter inter-planar energetics in such a way as to stabilize hexagonal stacking relative to rhombohedral stacking, resulting in a high density of stacking faults.

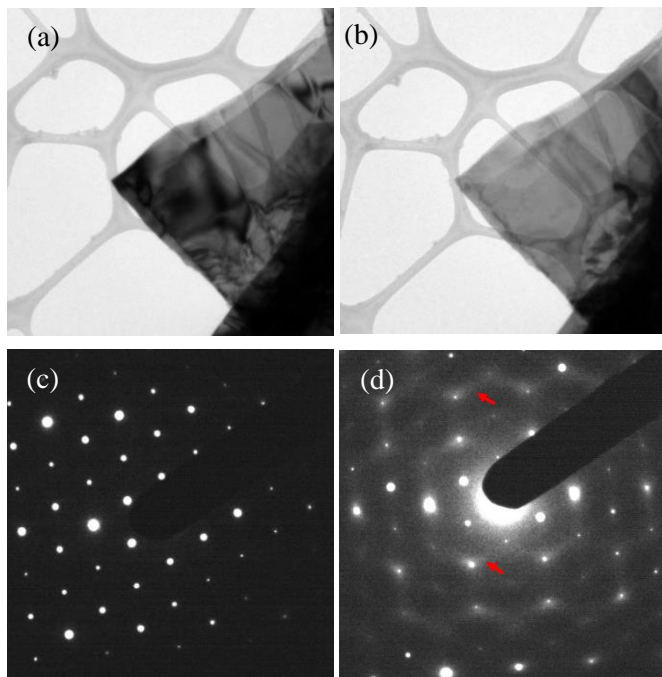


**Figure 2** (a), (b) Bright field TEM on a flake obtained from single crystal  $\text{Bi}_2\text{Se}_3$ . (c), (d) Selected Area Electron Diffraction from the corresponding areas shown in (a) and (b). The images in (a) and (c) show results when the beam is on [001] axis. Images in (b) and (d) show off-axis electron diffraction, for which the sample was tilted slightly (less than 5 degrees) away from the zone axis, arrows indicating examples of the diffused regions.

The process of self-intercalation has previously been discussed by other authors [32, 33]. Rietveld fitting of X-ray diffraction (XRD) on our  $\text{Bi}_2\text{Se}_3$  samples reveals that the  $a(=b)$  axis value is  $4.14 \text{ \AA}$ ,

which agrees with other reports. However, we find that our  $c$ -axis value is  $28.66 \text{ \AA}$ . This is  $0.02 \text{ \AA}$  higher than the  $28.64 \text{ \AA}$  reported in most previous experiments on  $\text{Bi}_2\text{Se}_3$  indicating Bi self-intercalation or the existence of Se vacancies. Previous authors [32] have discussed that a longer  $c$ -axis, with values as high as  $28.65 \text{ \AA}$ , can arise from the unintended intercalation of Bi into the van der Waals gap as a neutral metal  $\text{Bi}_2$  layer. Analysing the XRD peak broadening based on the Williamson-Hall analysis method [34, 35], presented in the supplemental materials, demonstrates lattice strain in our  $\text{Bi}_2\text{Se}_3$  sample. The measured isotropic strain is consistent with point defects, and further supports our assertion of Bi intercalation or Se vacancies. Based on the higher  $c$ -axis value in our samples, and our evidence for stacking faults in SAED, we suggest that the van der Waals gaps in our  $\text{Bi}_2\text{Se}_3$  crystals have zero-valent Bi or Se metal resulting from “self-intercalation.” The consequences of this are discussed in the later part of the paper.

The images in Figure 2(c), 2(d) correspond to the areas shown in Figures. 2(a), 2(b), respectively. As can be seen in Figure 2(d), the diffraction pattern with the crystal tilted slightly off the [001] zone axis yields diffuse streaks between the diffraction spots. As discussed in previous reports on other similar layered compounds [27, 28, 36-39], our interpretation is that this diffuse intensity is due to Periodic Lattice Distortion (PLD) associated with an incommensurate charge density wave (I-CDW), which often occurs as a precursor to a charge density wave (CDW) [27].

### 3.2 Resistivity Measurements

Four-probe DC resistivity measurements, shown in Figure 3 and Figure 4, were performed in the 2K-300K temperature range with linearly aligned electrodes on the  $ab$  surface of  $\text{Bi}_2\text{Se}_3$  single crystals, and with the electric field  $E \parallel ab$ . To ensure reproducibility, we performed measurements on several different pieces of as-grown single crystal. Figure 3(a), 3(b) are the results of different pieces from the same batch of as-grown single crystal. Resistivity measurements at zero field all show approximately metallic behavior from room

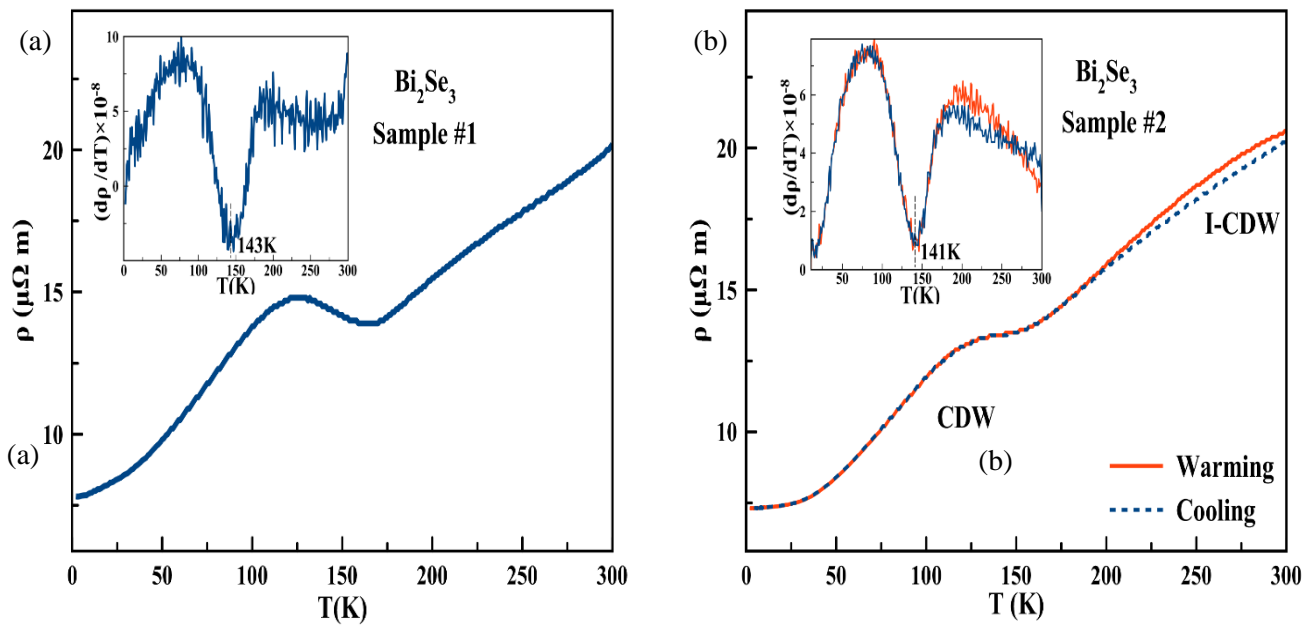


**Figure 3. Resistivity of  $\text{Bi}_2\text{Se}_3$  as a function of temperature for two different pieces, sample#1 and sample#2, measured in zero magnetic field with the electric field along the  $ab$  plane. (a) Measurement on sample #1 while cooling the sample from 300 K to 2 K; (b) Measurement on sample#2 for both cooling and heating. Insets for (a) and (b) are the plots of  $d\rho/dT$  as a function of temperature to clarify the temperature values of the inflection points and the potential CDW transition temperature  $T_{\text{CDW}}$ .**

temperature down to around 140K. Note a sharp upturn in resistivity with decreasing temperature, centered around 140K, followed by a return to metal-like behavior below 140K. In Figure 3(a), with cooling, we see a rise in resistivity from  $\sim 1.38 \times 10^{-5} \Omega\text{m}$  to  $1.47 \times 10^{-5} \Omega\text{m}$ ; in Figure 3(b), we observe a rise of  $\sim 1.31 \times 10^{-5} \Omega\text{m}$  to  $1.36 \times 10^{-5} \Omega\text{m}$ , followed in both cases by a return to metal-like behavior at lower temperature. The insets to Figure 3(a), 3(b) show  $d\rho/dT$  as a function of temperature, clarifying the inflection point and onset near 140K. We identify this metal-insulator like behavior as resulting from a gap or instability at the Fermi level, correlated with a transition to a possible CDW ground state [40, 41].

Heating and cooling cycles performed on the second piece of  $\text{Bi}_2\text{Se}_3$  shown in Figure 3(b) display very weak thermal hysteresis behavior above the onset transition temperature 140K, pointing to the possibility that the 140K transition is an unconventional second-order CDW transition [42, 43]. On the other hand, the hint of a thermal hysteresis (between heating and cooling) in resistivity above 200K, shown as a solid red line and a dashed blue line in Figure 3(b), points to the

presence of a possible first-order transition at higher temperature. We believe this could arise from a transition from a normal phase to an incommensurate charge density wave phase at some temperature above room temperature [44]. This agrees with our room-temperature electron diffraction data described below, in which we observe the evidence of PLD possibly associated with an I-CDW phase. The transition at 140K may then be associated with a second-order transition from I-CDW to CDW. The lack of (or, weak) thermal hysteresis at 140K indicates a possible phonon-mediated unconventional mechanism described further in the discussion section [1, 2, 45, 46].

Figure 4 examines the magnetic field dependence of the 140K transition for sample#2, the same sample as the one shown in Figure 1(b), with magnetic field  $H \parallel c$ -axis varying between 0.00T and 4.50T. The inset in Figure 4 displays  $d\rho/dT$  as a function of  $T$ , indicating that the transition temperature does not change with applied magnetic field  $H$  below 5T. This result is similar to the one obtained for an unconventional CDW in  $\text{La}_3\text{Co}_4\text{Sn}_{13}$

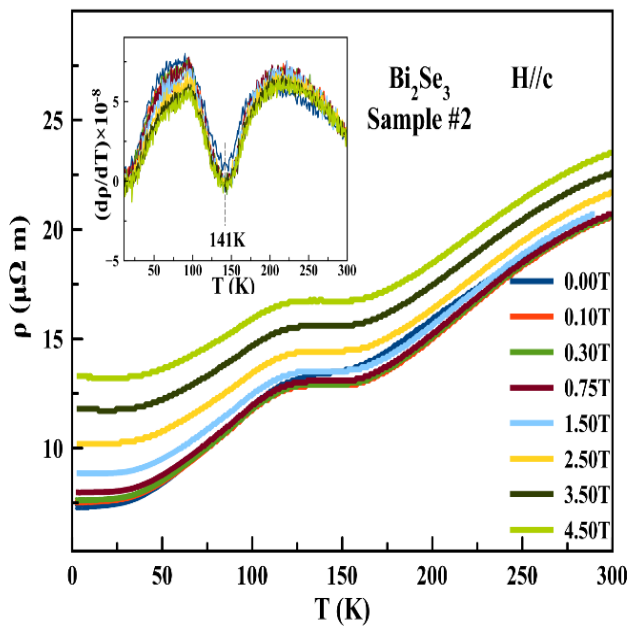


Figure 4. Thermal dependence of resistivity of  $\text{Bi}_2\text{Se}_3$  for different values of applied magnetic field  $H \parallel c$ -axis varying between 0.00 – 4.50 Tesla.

and is also consistent with our NMR results discussed in subsequent sections [42].

### 3.3 Nuclear Magnetic Resonance (NMR)

To provide microscopic information about the nature of these transitions, we performed NMR relaxation measurements. The nuclear spin-lattice relaxation rate  $1/T_1$  measures the recovery of the longitudinal nuclear magnetization following an external perturbation such as an RF field. The magnetization recovery  $M(t)$  is fitted with a stretched single exponential (see methods). However, we find that the fits with and without the stretch parameter give similar  $T_1$  results, giving stretched component  $\beta$  values close to 1. The results of this fit are shown in Figure 5. Figure 5 displays the temperature dependence of  $1/T_1$  of the central  $|\pm 1/2\rangle \leftrightarrow |\mp 1/2\rangle$  transition of the  $^{209}\text{Bi}$  nuclei ( $I = 9/2$ ), with temperature varying from 1.6K to 300K, pulse separation time  $\tau = 10\mu\text{s}$ , and with the external magnetic field  $H = 9.86\text{T}$  (frequency,  $f = 67.875\text{MHz}$ ) applied in two orientations,  $H \parallel c$ -axis and  $H \perp c$ -axis. It is clear that the spin-lattice relaxation rate  $1/T_1$  for both field orientations follows similar behavior as a function of temperature. Although the relaxation rates for  $H \parallel c$

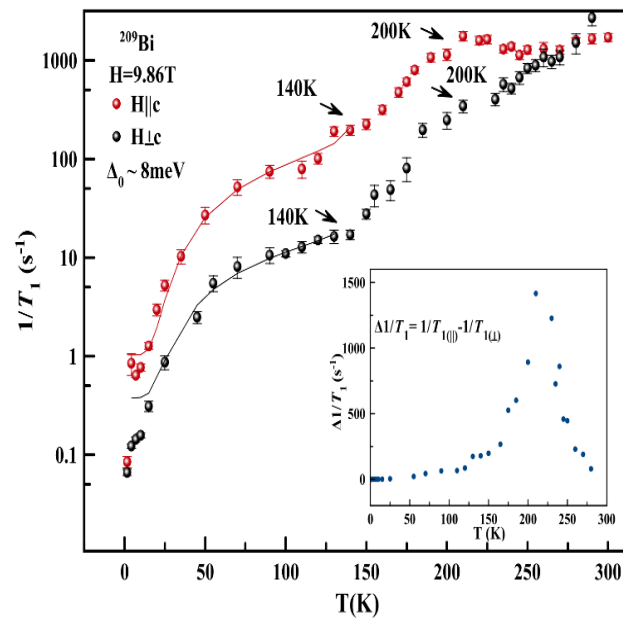


Figure 5. Spin-lattice relaxation rate ( $1/T_1$ ) shown with temperature  $T$  varying between 1.6K and 300K with applied magnetic field directions:  $H \parallel c$ -axis (red balls) and  $H \perp c$ -axis (black balls). Arrows indicate possible transitions at 140K, and 200K in each direction, where 140K is the possible commensurate CDW transition temperature. Solid lines are fits to a temperature-dependent CDW energy gap  $\Delta_0$ , with gap value of  $\sim 8\text{meV}$ . Inset: Differences of  $1/T_1$  from the two magnetic field orientations as a function of temperature where  $\Delta(1/T_1) = 1/T_1(\parallel) - 1/T_1(\perp)$ . We see the largest difference occurring at 200K.

are about an order of magnitude longer when compared to  $H \perp c$ , they approach nearly the same value at room temperature.

In Figure 5, we see two obvious slope changes: at 140K and at 200K, indicated by arrows. The 140K anomaly coincides with the metal-insulator transition observed in our resistivity measurements which we interpreted earlier as a transition to a possible commensurate CDW state. The sudden downturn of  $1/T_1$  below 140K suggests an energy gap opening associated with forming a CDW-like state below this temperature [47-50]. The  $T_1$  data is then fitted to a BCS-like gap equation, as shown in Figure 5. The obtained CDW gap value,  $\sim 8\text{meV}$ , is isotropic as it is independent of the direction of the magnetic field. The anomaly seen at 200K exhibits a weak anisotropy with the applied magnetic field. In the inset of Figure 5 we show the anisotropy of the relaxation rate,  $\Delta(1/T_1)$  as a function of

temperature. The anisotropy starts small at room temperature and grows as the temperature is lowered, peaking at 200K before decreasing again towards zero at base temperature. The following discussion section describes the 140K gap and 200K anomaly in more detail.

#### 4. Discussion

The exact nature of Fermi surface distortion, nesting, and density wave instability in a system such as  $\text{Bi}_2\text{Se}_3$  is critically dependent upon the details of its fermiology. Correlated electron systems typically exhibit intertwined electron ordered states resulting from several degrees of freedom such as lattice, charge, dimensionality, nematicity, and spin, all of which, in turn, tend to be strongly materials-dependent. Many properties of chalcogenides such as  $\text{Bi}_2\text{Se}_3$  arise from the nature of fluctuations, or overlaps in order parameter, among such intertwined orders. The severity of the overlap tends to be materials-dependent as well. Below, we discuss how material aspects of  $\text{Bi}_2\text{Se}_3$ , specifically, can lead to multiple ground states such as that of a charge density wave (CDW).

Further, the proximity of superconductivity and density wave orders in many materials begs a discussion of the observed CDW in the context of superconductivity in  $\text{Bi}_2\text{Se}_3$ , which we think is critical to understand the charge order, superconductivity, as well as nematicity in these families [51]. In this section, we begin with a discussion of the two different transitions found in our measurements. We end by describing important materials considerations that, we believe, drive the multiple (possibly intertwined) order parameters in this layered chalcogenide.

##### 4.1 Anomaly near 140K

Nuclear relaxation measurements, in Figure 5, together with resistivity measurements in Figure 3 and Figure 4, reveal a novel anomaly near 140K. We interpret this as a transition to a possible CDW state below 140K. We support this conclusion from electron diffraction measurements at room temperature (Figure 1 and Figure 2), which reveal the evidence of a periodic lattice distortion (PLD)

combined with diffuse scattering in off-axis diffraction, suggesting the presence of an incommensurate charge density wave (I-CDW) state already at room temperature. Interestingly,  $T_1$  anomalies have been associated with CDW-like transition in layered systems [47-50].

Below 140K, the CDW gap may be determined from the relaxation rate, as follows [52, 53]:

$$1/T_1 = a \exp[-\Delta(T)/T] + c \quad (2)$$

where we shall use the form of a T-dependent BCS gap equation:

$$\Delta(T) = \Delta_0 \tanh\left(1.74 \sqrt{\frac{T_c}{T} - 1}\right) \quad (3)$$

Here,  $T_c = T_{\text{CDW}}$  is the CDW transition temperature, and  $a$  and  $c$  are fitting constants. The fit (Figure 5) yields a zero-temperature energy gap of  $\Delta_0 = 8 \pm 2 \text{ meV}$  in both directions of the applied field. We estimate our coupling constant  $\lambda = \Delta_0/k_B T_{\text{CDW}} = 0.7$  (where  $T_{\text{CDW}} = 140 \text{ K}$  and  $k_B$  is the Boltzmann constant) which is close to the weak coupling limit. In the weak coupling limit, coupling constant  $\lambda \sim 1.7$ .

Previous relaxation measurements show a large variation in magnitudes and temperature dependences across samples prepared using various methods [54, 55]. These variations were attributed partly to the defects associated with Se-vacancies, which could shift the Fermi level by partially occupying the conduction band. Unlike previous studies, our data shows a very strong temperature dependence from 1.6 to 300K, spanning almost four orders of magnitude for H.c. (see Figure 6- all  $T_1$  data). The low-temperature behavior (below 50K) is comparable to that of sample #2 of Ref. [55] which the authors identify as the sample with higher carrier concentration.

Further, a comparison of the resistivity data (Figure 7-composite plot of  $\rho$  from ref. Young and this work) shows that our sample has slightly fewer carriers than Young's sample #2 but is far from insulating, suggesting that the Fermi level sits lower in the conduction band. This is consistent with our NMR Knight shift, whose values lie between Young's samples #2 and #3. For example, our  $K_{\text{iso}}$

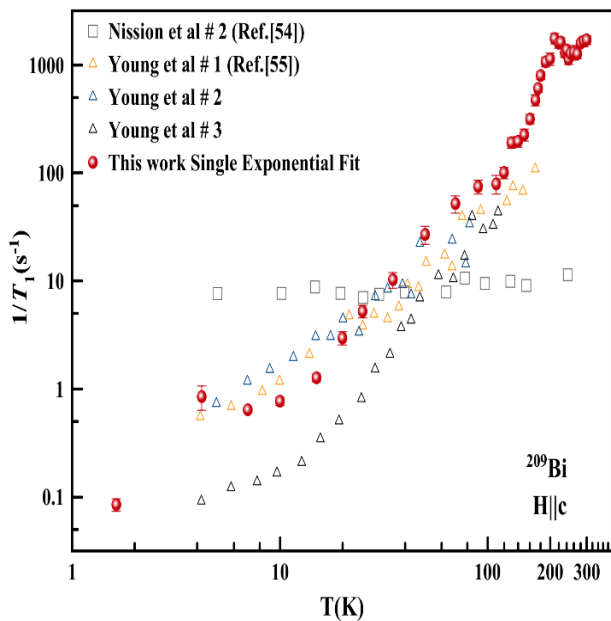


**Figure 6.** Comparison of Spin-lattice relaxation rates of  $^{209}\text{Bi}$  versus temperature from earlier published papers to our results in the magnetic field  $H \parallel c$  direction. The open data points are reproduced from Ref. [54] (square shapes from Nission’s sample #2, most of Nission’s results are in the same range) and Ref. [55] (triangle shapes, sample #1, #2 and #3). Solid data points are our results the same as displayed in Figure 5  $H \parallel c$  direction data, with a single exponential fit.

is  $\sim 0.4\%$ , while Young’s #2 is  $\sim 0.65\%$  and Young’s #3 is  $\sim 0.34\%$  at 4.2K. An argument can be made that it is possible that in some direction of the reciprocal space that half band-filling, essential for Peierls transition, has been serendipitously achieved in our sample by appropriate doping through Se-vacancies leading to the formation of CDW in our sample but not in others.

#### 4.2 NMR Anomaly near 200K

The NMR anomaly near 200K merits further discussion in light of the fact that the Debye temperature is  $\Theta_D \approx 182\text{K}$  for  $\text{Bi}_2\text{Se}_3$  [56]. Given that the behavior of  $1/T_1$  depends on the details of the high-temperature phonon spectrum, one would expect it to behave differently above and below the Debye temperature. Thus, it is possible that the transition observed around 200K in Figure 5 is due to changes in the phonon spectrum across  $\Theta_D$ . However, note the anisotropy in this transition with the direction of the applied magnetic field,  $H \parallel c$  and  $H \perp c$ , as is clear from Figure 5

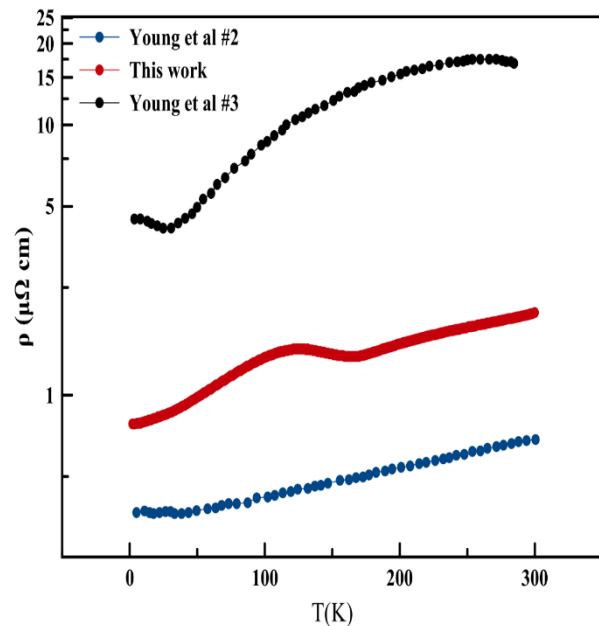


**Fig. 7.** Comparison of resistivity vs. temperature results from our transport measurement (red) and Ref. [54] Young et al. (sample #2 blue and sample #3 black).

In Figure 3(b), we observe a thermal hysteresis in resistivity above 182K. Whereas a transition across  $\Theta_D$  would yield a change in slope of resistivity, we are hard-pressed to explain the thermal hysteresis in resistivity, for  $T > 182\text{K}$ , based purely on a Debye temperature transition. On the other hand, a hysteresis between heating and cooling is often observed below a first-order I-CDW to CDW transition. The absence of a thermal hysteresis, as in the case of  $\text{Lu}_5\text{Ir}_4\text{Si}_{10}$ , often leads to speculation that the transition either is of second order or has some “unconventional” origin [42, 43]. In our case, as shown in Figure 3b, the resistivity below 140K does not display a thermal hysteresis. This indicates that the 140K transition is likely a second-order CDW transition. According to this reasoning, the 200K transition is a first-order transition.

Note in Figure 5 that the  $1/T_1$  data for both orientations follow similar behavior as a function of temperature, except that the relaxation rates for  $H \parallel c$  are about an order of magnitude faster compared to  $H \perp c$ . However, they approach almost the same value at room temperature. Above 200K, the temperature behavior differs: the  $1/T_1$  value remains



constant from room temperature to 200K for the parallel case while it precipitously drops for the perpendicular case. This would imply a constant relaxation mechanism that only exists in the parallel direction and is weakly dependent on temperature, while in the perpendicular direction, this mechanism monotonically diminishes until the temperature reaches 200K. The origin of this mechanism is not clear, but it may be related to the topological nature of this family of systems which suppresses the relaxation channel when the field is applied parallel to the plane of the layers [56, 57].

To analyze this further, let us suppose that the relaxation rates can be separated into electronic and phonon contributions [55]:

$$1/T_1(k) = 1/T_1^{\text{el}}(k) + 1/T_1^{\text{ph}}(k) \quad (4)$$

where  $k = \parallel, \perp$  are the magnetic field directions with respect to the crystal  $c$ -axis. The electronic contribution is magnetic in nature and is due to the spin scattering of the conduction electrons. On the other hand, the phonon contribution is driven by changes in the lattice which works its way to the nuclear relaxation via quadrupolar effects. Since the CDW energy gap we obtained below 140K is isotropic, it is reasonable to assume that the conduction band electronic contribution  $1/T_1^{\text{el}}(k)$  is also isotropic, as well as the temperature dependence of  $1/T_1^{\text{el}}(k)$  itself. We plot in the inset of Figure 5 the differences in relaxation rates  $\Delta 1/T_1 = 1/T_1(\parallel) - 1/T_1(\perp)$  between each field orientation. Here, we can clearly see that the anisotropy in relaxation is mainly due to phonon contribution along the  $H \parallel c$  direction, i.e.,  $\Delta 1/T_1 > 0$  at all temperatures. It starts small at room temperature, peaks at 200K, and finally freezes as

the sample is further cooled.

The positive value of  $\Delta 1/T_1$  reveals that a stronger lattice vibration (phonons) is present in the  $H \parallel c$ -axis measurements. This can be understood from the 2D layered structure of this material, where Bi-Bi bonds within the  $ab$  planes have stronger electron-phonon coupling effects than the ones along the  $c$ -axis [58]. These results are as expected since the longitudinal relaxation  $1/T_1(\parallel)$  is sensitive to fluctuations perpendicular to the direction of the

magnetic field. Combining our high-temperature observations from SAED and resistivity data, the  $\Delta 1/T_1$  peak at 200K, is likely a phonon-mediated structural phase transition. At high temperatures, the temperature-dependent behavior of  $1/T_1$  is driven by its correlation with the lattice imperfections or the PLD. When the temperature reaches 200K, the lattice vibration becomes weak and a soft phonon is observed, resulting in a structural phase transition and a peak in relaxation. This is reminiscent of critical slowing down in spin systems where a peak in  $1/T_1$  is observed when the system undergoes a phase transition. From 200K to 140K, the electronic contribution becomes dominant and the phonon vibrations are further weakened. However, phonon vibrations are not entirely absent and still contribute to the relaxation. In this range, some electronic charges are ordered with the underlying lattice, and some are not; thus, there is a mixture of I-CDW and CDW phases. Since  $1/T_1$  is an integration over the entire Fermi surface, it is possible that in this temperature range the Fermi surface only opened a small segment with mini CDW gaps. At 140K, a threshold is reached when the phonons are weak enough and the electronic charges become more commensurate with the underlying lattice. Consequently, the entire Fermi surface undergoes a gapped Peierls transition, thus completing the CDW-like state.

#### 4.3 Materials Considerations

Most CDW occurs in quasi-1D or quasi-2D; our current understanding of CDW only includes some of the complexities involved in the 3D case, where electron correlations are thought to play a primary role [59]. In this context, it is instructive to discuss further the possible effect of intercalation on  $k_F$  anisotropy between  $k_z$  versus  $k_x, k_y$ . Xiangang and Sergey [1] suggest that small changes in the position of Bi in the  $z$ -direction can modify the nesting vector  $X(q) = \sum \delta(\epsilon_k) \delta(\epsilon_{k+q})$ , where,  $\epsilon_k$  and  $\epsilon_{k+q}$  are the energy of states at/near the Fermi level. This nesting vector is largest for wavevector  $q$  along the  $\Gamma_z$  direction, when  $q$  is close to zero. This can lead to strong Fermi surface nesting, and strong electron-phonon coupling. Displacement along [001] at small  $qs$  (i.e., small momenta) breaks spatial

inversion symmetry, lifts double degeneracy, and leads to a large electron-phonon coupling matrix element along this direction close to the zone center. Further calculations by Xiangang and Sergey [1] and neutron scattering experiments by J. Wang *et al.* [2] show broad phonon linewidths for small  $qs$ , which could dominate electron-phonon coupling. Based on these arguments, we tentatively pose the possibility of the presence of a quasi-1D Peierls-type transition in the  $z$ -direction of  $\text{Bi}_2\text{Se}_3$ .

The somewhat elusive nature of superconductivity in single crystals of  $\text{Cu-Bi}_2\text{Se}_3$ , especially the variability of superconducting fraction and  $T_c$  to quenching temperature [25, 26], is likely due to the high sensitivity of electron interactions to actual conditions of quenching and growth. The crystals discussed here were grown using a standard self-flux method, and a quenching temperature of 650C. The ideal topological insulator,  $\text{Bi}_2\text{Se}_3$ , has separate bulk and surface states. However, experimentally, intrinsic defects and disorders can be widely found in  $\text{Bi}_2\text{Se}_3$  and intercalated/electron-doped  $\text{Bi}_2\text{Se}_3$  [9, 41]. Schneeloch *et al.* [26] used different growth conditions to grow Cu-doped  $\text{Bi}_2\text{Se}_3$  superconductor and reported that high temperature quenching (above 560C) is essential for superconductivity, especially superconductivity with high diamagnetic shielding fraction. Other growth conditions either cause no SC or show weak diamagnetic shielding fraction. This is also our observation [25] in  $\text{Cu-Bi}_2\text{Se}_3$ . Schneeloch *et al.* suggest that the quenching process helps maintain either a primary intercalated phase or a secondary phase responsible for superconductivity. Huang *et al.* show that high annealing temperature ( $\sim 600\text{C}$ ) can cause intercalation of  $\text{Bi}_2$  in  $\text{Bi}_2\text{Se}_3$  [46]. Our results in this article indicate that high-temperature quenching (from above 650C) leads to strong electron and lattice order, and interesting electronic ground states such as a CDW or superconductivity.

X-ray diffraction (XRD) on powdered samples reveals that the  $a$ -axis value of our single crystal  $\text{Bi}_2\text{Se}_3$  agrees with those of most other reports, but that the  $c$ -axis, at 28.66 Å, is 0.02 Å higher than the 28.64 Å reported in most previous reports  $\text{Bi}_2\text{Se}_3$  [32, 60, 61]. Huang *et al.* assert that a longer  $c$ -axis

arises from unintentionally doped Bi-rich flux growth of  $\text{Bi}_2\text{Se}_3$  where Bi forms a neutral metal  $\text{Bi}_2$  layer intercalated into the van der Waals gap [32]. They also show that crystals with patches of intercalated Bi show high  $c$ -axis values of up to 28.65 Å, close to the  $c$ -axis value of 28.66 Å obtained from our Rietveld refinement. XRD results on our  $\text{Bi}_2\text{Se}_3$  single crystals show no signs of the formation of metastable phases of staged  $(\text{Bi}_2)_m(\text{Bi}_2\text{Se}_3)_n$ . The solidification temperature of  $\text{Bi}_2\text{Se}_3$  (705 C) is higher than the melting point of both pure Bi (271.4 C) and pure Se (220 C). Additionally, Se is a vapor above 685 C, below the solidification temperature of  $\text{Bi}_2\text{Se}_3$ . Consequently, the stoichiometry of  $\text{Bi}_2\text{Se}_3$  forming at the liquid-vapor interface can be highly dependent upon the vapor pressure of Se at 705 C. For high annealing temperatures (around 600 C), partial decomposition might occur. Huang presumes that this is due to a large number of Se vacancies created in an evacuated environment, resulting in liquid Bi in the flux ending up in the van der Waals gaps rather than incorporating into a Bi-Se quintuple layer containing Se vacancies. Our crystals quenched at 650 C (above the high annealing temperature of 600 C that Haung claims results in Se vacancies) could lead to Se vacancies and intercalated Bi. We surmise that, as there is not enough excess Bi to form the metastable phase of staged  $(\text{Bi}_2)_m(\text{Bi}_2\text{Se}_3)_n$ , excess Bismuth in our crystals forms randomly distributed  $\text{Bi}_2$  inter-layers in the crystal. The resulting Bi-chains could help form a quasi-1D Peierls-type transition or a quasi-2D type CDW [32, 59, 62]. In summary, specific growth conditions can drive the observation of a CDW or superconductivity in  $\text{Bi}_2\text{Se}_3$ . Further work is needed in this direction.

In addition to the discussion of Figure 7, a comparison of our temperature-dependent resistivity data and Knight shift of central transition with Young's sample #2 and sample #3 further supports that crystal growth conditions have important impact on the electronic behavior of samples. All three samples (ours, Young's #2, and #3) were grown under different conditions. Young's ARPES results show that the Fermi level of their sample #2 lies within the bottom of the conduction

band and that of sample #3 lies in the surface state, far below the conduction band. Since both our resistivity data and Knight shift values are in between Young's two samples (but closer to #2), it is likely that the Fermi level of our sample sits close to but lower than the Fermi level of their sample #2.

## 5. Conclusion

To conclude, we show a phase transition at 140K in high-temperature quenched Bi<sub>2</sub>Se<sub>3</sub>. We suggest that it is compatible with a possible charge density wave (CDW) order in Bi<sub>2</sub>Se<sub>3</sub>. Diffuse streaks in SAED measurements indicate the presence of an incommensurate periodic lattice distortion at room temperature, reminiscent of an incommensurate charge density wave (I-CDW). A metal-to-insulator-like transition at 140K in resistivity measurements indicates the opening of a CDW-like energy gap. NMR spin-lattice relaxation rate  $1/T_1$  measurements further confirm the presence of the 140K transition with an energy gap of about 8meV. Using this, together with thermal hysteresis studies of resistivity, we conclude that Bi<sub>2</sub>Se<sub>3</sub> displays a possible unconventional second-order quasi-1D CDW transition temperature at 140K.  $1/T_1$  also reveals another anomaly near 200K, which shows an anisotropy in comparison of H<sub>||</sub>c to H<sub>⊥</sub>c measurements.

## Author Contributions

YL and CP grew samples. Electron diffraction was performed by YL and MAS, led by MAS. YL and SR performed NMR measurements under the direction of AR; CP and AD assisted YL in analysis. CP did the Williamson-Hall Analysis in supplemental materials. YL wrote the first draft of the manuscript under the direction of PG, with assistance from AR, CP and AD and reviewed by AR. PG provided supervision of the overall project.

## Acknowledgments

We gratefully acknowledge support from Steve Hardcastle of the Advanced Analysis Facility, and Prof. M. Gajdardziska-Josifovska for the use of the Hitachi H-9000NAR high-resolution transmission electron microscope in the HRTEM facility. We acknowledge an earlier AFOSR MURI grant to PG.

A portion of this work was performed at the National High Magnetic Field Laboratory, which is supported by the National Science Foundation Cooperative Agreement No. DMR-1644779 and the state of Florida.

## References

- [1] X.Wan and S. Savrasov, *Nat Commun* **5**, 4144 (2014).
- [2] J. Wang *et al.*, *Nat Commun* **10**, 2802 (2019).
- [3] B. J. Lawson *et al.*, *Phys. Rev. B* **94**, 041114(R) (2016).
- [4] M. Hecker and J. Schmalian, *npj Quant Mater* **3**, 26 (2018).
- [5] K. Matano *et al.*, *Nature Phys* **12**, 852–854 (2016).
- [6] J. Shen *et al.*, *npj Quant Mater* **2**, 59 (2017).
- [7] Y. Xia *et al.*, *Nature Phys* **5**, 398–402 (2009).
- [8] D. Hsieh *et al.*, *Nature* **460**, 1101–1105 (2009).
- [9] Y. S. Hor *et al.*, *Phys. Rev. B* **79**, 195208 (2009).
- [10] M. A. Tumelero, R. Faccio, and A. A. Pasa, *J. Condens. Matter Phys.* **28**, 425801 (2016).
- [11] E. Lahoud *et al.*, *Phys. Rev. B* **88**, 195107 (2013).
- [12] K. Kirshenbaum *et al.*, *Phys. Rev. Lett.* **111**, 087001 (2013).
- [13] S. Sasaki *et al.*, *Phys. Rev. Lett.* **107**, 217001 (2011).
- [14] T. Asaba *et al.*, *Phys. Rev. X* **7**, 011009 (2017).
- [15] Y. Kohama *et al.*, *J. Phys. Soc. Jpn.* **77**, 094715 (2008).

- [16] T. Kiss *et al.*, *Phys. Rev. Lett.* **94**, 057001 (2005)
- [17] G. R. Stewart, *Adv. Phys.* **66**, 75-196 (2017).
- [18] J. C. S. Davis and D.-H. Lee, *Proc. Natl Acad. Sci. USA* **110**, 17623–17630 (2013).
- [19] D. Biswas, *S. Sci Rep* **5**, 17351 (2015).
- [20] Y. S. Hor *et al.*, *Phys. Rev. Lett.* **104**, 057001 (2010).
- [21] K. Kuroda *et al.*, *Phys. Rev. Lett.* **105**, 076802 (2010).
- [22] L. Fu, *Phys. Rev. Lett.* **103**, 266801 (2009).
- [23] H. Zhang, C.-X. Liu, and S.-C. Zhang, *Phys. Rev. Lett.* **113**, 066801 (2013).
- [24] K. J. Koski *et al.*, *JACS* **134**, 13773–13779 (2012).
- [25] N. P. Smith, Ph.D. Thesis, University of Wisconsin Milwaukee (2018).
- [26] J. A. Schneeloch, R. D. Zhong, Z. J. Xu, G. D. Gu, and J. M. Tranquada, *Phys. Rev. B* **91**, 144506 (2015).
- [27] J. A. Wilson, F. J. Di Salvo, and S. Mahajan, *Adv. Phys.* **24** 117–201(1975).
- [28] J. A. Wilson, F. J. Di Salvo, and S. Mahajan, *Phys. Rev. Lett.* **32** 882 (1974).
- [29] A. Narath, *Phys. Rev.* **162**, 320 (1967).
- [30] A. Suter, M. Roos, J., Brinkmann and D. Mixed, *J. Phys: Condens. Matter*, **10**, 5977-5994 (1998).
- [31] M. Wang and K. J. Koski, *J. Phys. Condens. Matter* **28**, 494002 (2016).
- [32] F.-T. Huang *et al.*, *Phys. Rev. B* **86**, 081104(R) (2012).
- [33] J. Dai *et al.*, *Phys. Rev. Lett.* **117**, 106401(2016).
- [34] D. Nath, F. Singh, and R. Das, *Mater. Chem. Phys.* **239**, 122021 (2020).
- [35] P. M. Shafi and A. C. Bose, *AIP Advances* **5**, 057137 (2015).
- [36] P. M. Williams, C. Scruby, W. Clark, and G. Parry, *J. Phys. Colloques.* **37** C4-139–150(1976).
- [37] W. L. McMillan, *Phys. Rev. B* **12** 1187 (1975).
- [38] F. J. Di Salvo and T. M. Rice, *Phys. Today* **32** 32 (1979).
- [39] Y. Li, N. P. Smith, W. Rexhausen, M. A. Schofield, and P. Guptasarma, *J. Phys. Mater.* **3** 015008 (2020).
- [40] G. Duvjir *et al.*, *Nano Letters* **18** (9), 5432-5438 (2018).
- [41] R. A. Craven and S. F. Meyer, *Phys. Rev. B* **16**, 4583 (1977).
- [42] J. Welsch *et al.*, *Phys. Rev. Materials* **3**, 125003 (2019).
- [43] Y.-K. Kuo *et al.*, *Phys. Rev. B* **64**, 125124 (2001).
- [44] A. Zong *et al.* *Sci. Adv.* **4**, 5501 (2018).
- [45] J. V. Wezel, P. Nahai-Williamson, and S.S. Saxena, *Phys. Rev. B* **81**, 165109 (2010).
- [46] K. Sugawara *et al.*, *ACS Nano* **10**, 1341 (2015).
- [47] C. Berthier, D. Jérôme, and P. J. Molinié, *Phys. C: Solid State Physics*, **11**, 797 (1978).
- [48] T. Ohno, Y. Kishimoto, and K. Miyatani, *Physica B (Amsterdam)* **230**, 988 (1997).

- [49] T. Tsuda, Y. Kitaoka, and H. Yasuoka, *Physica B+C (Amsterdam)* **105**, 414 (1981).
- [50] S. Wada, H. Alloul, and P. Molinié, *J. Physique Lett.* **39**, 243-247 (1978).
- [51] J. C. Séamus Davis and D.-H. Lee, *PNAS*. **110**, 17623-17630 (2013).
- [52] M. Yogi, N. Higa, H. Niki, T. Kawata, and C. Sekine, *J. Phys.: Conf. Ser.* **683**, 012030 (2016).
- [53] G. Gruner, *Rev. Mod. Phys.* **60**, 1129-undefined (1988).
- [54] D. M. Nisson *et al.*, *Phys. Rev. B* **87**, 195202 (2013).
- [55] B.-L. Young *et al.*, *Phys. Rev. B* **86**, 075137 (2012).
- [56] V. Fal'ko and T. Jungwirth, *Phys. Rev. B* **65**, 081306 (2002).
- [57] A. A. Taskin *et al.*, *Nat Commun* **8**, 1340 (2017).
- [58] X. Zhu *et al.*, *Phys. Rev. Lett.* **108**, 185501 (2012).
- [59] X. Zhu, Y. Cao, J. Zhang, E. W. Plummer, and J. Guo, *Proc. Natl Acad. Sci. USA* **112**, 2367–2371 (2015).
- [60] O. Chiatti *et al.*, *Sci Rep* **6**, 27483 (2016).
- [61] G. Martinez *et al.*, *Sci Rep* **7**, 6891 (2017).
- [62] X. Zhu, J. Guo, J. Zhang, and E.W. Plummer, *Adv. Phys.: X*, **2**, 622-640 (2017).